FLOW CHARACTERISTICS OF TWO-PHASE DISPERSED ANNULAR STREAMS IN HEATED TUBES

B. I. Nigmatulin

UDC 532.529.5

Patterns and characteristics of flow through heated tubes are investigated on the basis of concepts of two-phase dispersed annular flow patterns [1] within the framework of the three-velocity and single-temperature equilibrium model, with flowrates of the mixture not too close to critical. Conditions for onset of burnout of the second kind, i.e., deterioration in the transfer of heat leading to an abrupt rise in the temperature of the heating surface, and, as such, associated with desiccation of the thin film of liquid on the wall [2, 3], are investigated. Hydraulic drag, the flowrate of liquid in the film, and the true steam content by volume are among the factors discussed. Two-phase flow patterns in dispersed annular flow are characterized by the combined motion of the three components of the mixture: vapor, the liquid wall film, and droplets. The assumption entertained is that each component of the mixture acquires its own velocity, and that the temperature of the mixture is equal, in each cross section through the channel, to the saturation temperature at the pressure prevailing in the particular cross section.

1. Basic Equations

We begin by considering the motion of a dispersed annular stream through a cylindrical tube. According to our earlier article [1], we can state the differential equations of conservation of mass and of momentum in the projection onto the axis of this cylindrical tube for each component of the mixture, plus the thermal balance equation for the mixture as a whole. Further, parameters referable to the vapor, liquid film, and droplets are designated consistently below by the respective subscripts 1, 2, 3:

$$\frac{dm_1}{dz} = J_{21} - J_{12} + J_{31} - J_{13}, \quad \frac{dm_2}{dz} = J_{12} - J_{21} + J_{32} - J_{23},$$

$$\frac{dm_3}{dz} = J_{13} - J_{31} + J_{23} - J_{32}$$

$$m_1 \frac{du_1^u}{dz} = -\alpha F_1 \frac{dp}{dz} - \rho_3 F_1 f - f_{12} + J_{21}(u_{21} - u_1^u) +$$
$$+ J_{12}(u_1^u - u_{12}) + J_{31}(u_{31} - u_1^u) + J_{13}(u_1^u - u_{13}) - \rho_1 F_1 g$$

$$m_2 \frac{du_2^u}{dz} = F_2 \frac{dp}{dz} + f_{12} - f_w + J_{21}(u_2^u - u_{21}) + J_{12}(u_{12} - u_2^u) + \quad (1.1)$$
$$+ J_{32}(u_{32} - u_2^u) + J_{23}(u_2^u - u_{23}) - \rho_2 F_2 g$$

$$m_3 \frac{du_3^u}{dz} = -(1-\alpha) F_1 \frac{dp}{dz} + \rho_3 F_1 f + J_{13}(u_{13} - u_3^u) +$$
$$+ J_{31}(u_3^u - u_{31}) + J_{23}(u_{23} - u_3^u) + J_{32}(u_3^u - u_{32}) - \rho_3 F_1 g$$

$$\frac{d}{dz}\left\{\sum_{j=1}^{3} m_j \left(e_j + \frac{p}{\rho_j^\circ}\right)\right\} = Q_w = \pi D q_w$$

$$\left(m_j = \int_{F_j} \rho_j u_j \, dF, \quad m_j u_j^u = \int_{F_j} \rho_j u_j^2 \, dF, \quad m_j e_j = \int_{F_j} e_j \rho_j u_j \, dF\right.$$

$$\left.\rho_1 = \rho_1^\circ \alpha, \quad \rho_2 = \rho_2^\circ, \quad \rho_3 = \rho_3^\circ (1-\alpha)\right)$$

Moscow. Translated from Zhurnal Prikladnoi Mekhaniki i Tekhnicheskoi Fiziki, No. 4, pp. 78-88, July-August, 1973. Original article submitted January 22, 1973.

Here m_j (j = 1, 2, 3) is the flow of mass of the j-th component of the mixture through the transverse cross section of the channel, such that $m_1 + m_2 + m_3 = m$, where m is the mass flowrate of the mixture; ρ_j, ρ_j°, u_j^m, and u_m^u are respectively the mean and true densities and the velocities referred to mean flowrate and to mean momentum; α is the steam content by volume in the core of the flow; $F_1(z)$ and $F_2(z)$ are the respective portions of the cross-sectional area presented by the channel that are occupied by the flow core and by the liquid film, such that $F_1(z) + F_2(z) = F$, where F is the area of the channel transverse cross section; J_{kj} (k, j = 1, 2, 3; $k \neq j$) are the intensities of the mass-transfer processes occurring between the k-th and j-th components of the mixture; u_{kj} (k, j = 1, 2, 3; $k \neq j$) are the velocities at the interface between the components of the mixture; f is the coupling force between the vapor and the droplets; f_{12} is the friction force acting on the film–vapor interface; f_w is the friction force operating between the liquid film and the solid wall of the channel; the last terms in the right-hand members of the momentum conservation equations are projections of the mass forces onto the z axis; e_j and e_j° are the mean and true internal energies, respectively, Q_w is the external incremental inflow of heat per unit time interval per unit channel length; q_w is the external incremental inflow of heat per unit time interval from a unit area of the channel surface.

The equations of state of the phases are set up in the form

$$p = \rho_1^\circ R T_s, \quad \rho_2^\circ = \rho_3^\circ = \text{const}, \quad T_1 = T_2 = T_3 = T_s$$
$$i_1(p, T_s) = i_2(p, T_s) + r(p), \quad i_2 = i_3 = c_2(T_s - T^\circ) + p / \rho_2^\circ$$

Here T_s is the equilibrium saturation temperature corresponding to p, i is the specific enthalpy, and r is the latent heat of vaporization.

Similarly as in [1], we obtain the relationship between parameters at the interface between the components of the mixture and the averaged characteristics of the flow pattern

$$u_{31} = u_{13} = u_3^u, \quad u_{12} = u_{21} = u_{23} = u_2', \quad u_{32} = u_3^u$$

where u_2' is the velocity of the liquid streaming over the film surface.

In the case of turbulent flow through the film and core of the stream, accurate to the order $0(n_j^2)$ and $0(n_2\delta/D)$, we have respectively

$$u_j^m = u_j^u = u_j \quad (j = 1, 2, 3), \quad u_2' = (1 + n_2) u_2^m$$

where n_j is the power exponent in the power distribution law of the velocity of the j-th component of the mixture over the tube radius, δ is the mean film thickness, and D is the tube inner diameter.

In laminar film flow, at numbers $R_2 < 300$ to 400, where $R_2 = u_2^m \delta / \nu_2$, ν_2 is the kinematic viscosity coefficient of the liquid

$$u_2^u = {}^4/_3 u_2^m, \qquad u_2' = 2 u_2$$

The expressions for f, f_{12}, f_w comprise the force couplings between components of the mixture, as stated in a manner similar to that followed in [1]

$$f = \frac{3}{4} \frac{\rho_1^\circ}{\rho_2^\circ} \frac{C_{13}}{d} \frac{(u_1 - u_3)^3}{|u_1 - u_3|} \quad \left(C_{13} = C_{13}(R_{13}, \alpha), \quad R_{13} = \frac{|u_1 - u_3| d}{\nu_1} \right)$$

where d is the droplet diameter, and ν_1 is the kinematic viscosity coefficient of the vapor

$$f_{12} = {}^1/_2 C_{12} \pi D_1 \rho_1^\circ (u_1 - u_2')^2, \quad C_{12} = C_{12}(\delta / D, R_1, R_2)$$
$$R_1 = (u_1 - u_2') D_1 / \nu_1, \quad D_1 = D - 2\delta$$
$$f_w = \pi D \rho_2^\circ (u_2^m)^2 / 2, \quad C_w = C_w(R_2, \delta / D)$$

The process by which moisture is removed from the film surface in the heated tube can proceed in response to two causal factors: first, moisture can be dislodged from the crests of large-scale perturbing waves (dynamical stripping); second, in the case of bubble boiling behavior in the film, liquid droplets can be entrained together with the vapor bubbles into the core of the flow (bubble stripping) [4]. We then have

$$J_{23} = J_{23}^d + J_{23}^b$$

where J_{23}^{d} is the intensity of dynamical stripping, J_{23}^{b} is the intensity of bubble stripping. Each of these two distinct stripping processes obeys its own regularities, so that they have to be studied separately. We may note the following with respect to bubble stripping behavior: when the flow velocities are appreciably high, when the film velocity is great, suppression of boiling within the film becomes possible [5]. In the presence of bubbling, the intensity of bubble stripping behavior increases drastically as the external specific heat flux and the film thickness increase. It does not seem possible to estimate the effect of pressure, of the liquid flowspeed in the film, of the diameters of the vapor bubbles, etc., on the intensity of bubble entrainment, since experimental data on bubble entrainment are almost completely lacking. We shall assume that moisture entrainment from the surface of the film is determined for the most part by dynamical stripping, whereas the range of applicability of this assumption can be estimated when we compare the numerical and experimental data on the rates of liquid flow through the film in a heated tube and in an unheated tube, and the numerical and experimental data on burnout of the second kind. A linear relationship has been proposed [1] for the intensity of dynamical stripping:

$$\begin{aligned} &J_{23}^{d}[\pi D_1\rho_1^{\circ}(u_1-u_2')]^{-1}=A(W_2-W^*) \quad (W_2>W^*),\\ &J_{23}^{d}=0 \quad (W_2\leqslant W^*)\\ &A=\varkappa(\rho_2^{\circ}/\rho_1^{\circ})^n[(u_1-u_2')/u_2']^m, \quad W_2=\rho_2^{\circ}(u_2')^2\delta/\sigma_2 \end{aligned} \tag{1.2}$$

where W* is the Weber critical ratio characterizing the onset of dynamical stripping, W* = 20 to 50; $\varkappa$, n, and m are constants found from the empirical data.

In order to estimate the rate at which droplets settle onto the film in an unheated channel, J_{32}', we can resort to a semiempirical formula [6]

$$\begin{aligned} &J_{32}'=\pi D_1\rho_2^{\circ}(1-\alpha)\,v_{31}=0.0817\;D_1\rho_2^{\circ}[(1-\alpha)/\alpha](u_3-u_2')R_{32}^{-0.25}\\ &R_{32}=D_1(u_3-u_2')/\nu_1 \end{aligned} \tag{1.3}$$

Here v_{31} is the velocity of the droplets relative to the vapor in the transverse direction. Assuming, in a first approximation, that the relative velocity v_{31} can be estimated on the basis of Eqs. (1.3) in the case where transverse flow exists from a film (heated tube), we get

$$\begin{aligned} &J_{32}=J_{32}'-\eta J_{21}(1-\alpha)(\rho_2^{\circ}/\rho_1^{\circ}) \quad (J_{32}'>\eta J_{21}(1-\alpha)(\rho_2^{\circ}/\rho_1^{\circ}))\\ &J_{32}=0, \quad J_{32}'\leqslant\eta J_{21}(1-\alpha)(\rho_2^{\circ}/\rho_1^{\circ}) \end{aligned} \tag{1.4}$$

Here η is an empirical constant which can be estimated from the interface marking off the flow pattern with droplets settling out on the film and the flow pattern free of such settling.

From the thermal balance equation for the entire mixture, for large p and large flowrates of the mixture that are not too close to critical, we have

$$J_{21}=Q_w/r, \quad J_{12}-J_{13}=J_{31}=0 \tag{1.5}$$

The system of equations (1.1) was integrated numerically (solving the Cauchy problem) with p, w, x_1, and x_2 fixed in the initial cross section, where $x_j = m_j/m$ and $x_1 + x_2 + x_3 = 1$, $w = m/F$ is the specific mass flowrate of the mixture. Usually, if this is not expressly stipulated, the parameters of the mixture in the equilibrium state [1], i.e., in a state of the mixture such that the stream parameters will undergo virtually no change at all downstream without heating, are accepted as the remaining initial data at the entry to the heated tube. Investigation of the special features of Eqs. (1.1) has shown that this equilibrium condition of flow without heating and low relative pressure losses in the channel $\Delta p \ll p$ corresponds to the nodal singularity of the system (1.1). The heating problem was continued further out to the channel cross section in which the liquid flowrate in the film vanished. This condition is taken as the condition of onset of burnout of the second kind. Experimental measurements of the rate of liquid flow in the film and of film thicknesses before the onset of burnout in water [7, 8] and in freon-12 [9] confirmed that assumption.

2. Some Results

Figures 1-7 display some results of numerical integration together with experimental data furnished by various authors in illustration of the effect exerted by p, w, x_1, D, and q_w on the basic characteristics of the dispersed annular two-phase flow pattern through a heated tube.

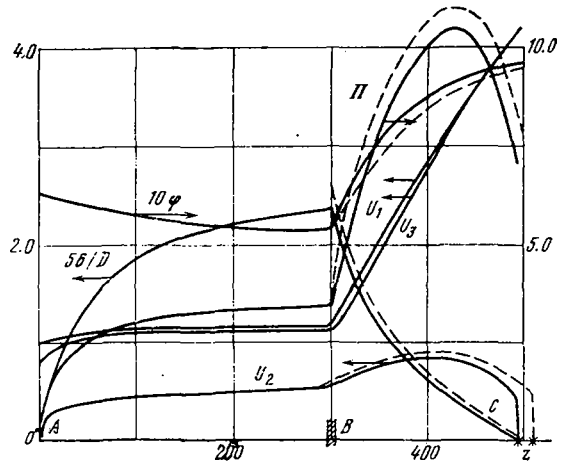

Fig. 1

Figure 1 shows an example of the results of calculating the characteristics of dispersed annular flow along a tube under inlet pressure p = 69 bar, w = 1080 kg/m^2 · sec, x_{10} = 0.1, x_{20} = 0.0, D = 10.2 mm. The subscript D denotes parameters of entry to the unheated section (AB for the stabilization section, BS for the heated section. The specific heat flux on the heated section $q_w = 7 \cdot 10^5$ W · m^{-2}. Here φ is the true steam content by volume in the mixture, $u_j = u_j/u_0$ (j = 1, 2, 3), Z = 2z/πD, Π is the relative pressure loss due to friction, and is equal to the ratio of pressure losses due to friction in two-phase flow to the pressure losses due to friction when water flows at saturation temperature and the same specific mass flow rate.

$$\Pi = \left[\frac{dp}{dz}\right]_f \Big/ \left[\frac{dp}{dz}\right]_{f0}$$

The friction factor in water flow through a smooth tube was taken according to the Blasius formula. It is clear from Fig. 1 that the system practically attains the equilibrium state on the AB interval. The continuous curves for the BC interval are arrived at when the parameters at inlet to the heated section correspond to the equilibrium state of the system, while the broken curves indicate the situation when virtually the entire liquid is concentrated in the cross section B and slip between vapor and film is 2, viz. the initial conditions in the experiments [8]. Clearly, in the second instance burnout (denoted here and in what follows by the asterisk, with x_2 = 0) is somewhat more extended than the set of conditions featuring equilibrium parameters at the inlet. The extent of agreement between numerical and experimental data [8] is discussed below. The dependence of Π on Z on the heated section stands out as the similarly experimentally determined dependence [10] based on the hydraulic drag in a long tube.

Figures 2 and 3 show examples illustrating comparison of both calculated and experimental burnout results. The experiments were staged on a direct-flow vertical test stand. After supercritical steam was throttled, the necessary steam content x_{10} at the inlet to the unheated section was arrived at, after which the equilibrium state of the mixture was attained. The mixture then entered the 1.5 m or 3 m long heated section. (The experiments over a 3-m-long experimental interval were carried out jointly with F.P. Lantsman.) The unheated and heated sections were of diameter D = 8 mm. The sequence in which the experiments were staged and the experimental arrangement are detailed in [2]. The critical vapor content x_{bn}, i.e., the value of x_1 at the site where the wall temperature rises abruptly on account of burnout brought on by the film drying out (x_2 = 0), was determined in the experiments as a function of the parameters p, w, q_w, and x_{10}. Figure 2 shows the correlation of empirical and theoretical data on a correlation of empirical and predicted data on x_{bn} as a function of x_{10} for different p and w values.

The empirical data points and curves 1, 2, 3 and 4 refer to p = 49 bar and respectively to w = 500, 1000, 1250, and 1900 kg · m^{-2} · sec^{-1}, $q_w = 4 \cdot 10^5$ to $1.5 \cdot 10^6$ W · m^{-2}. The empirical data points and curve 5 are obtained at channel inlet pressure 21 bar and at w = 1000 kg · m^{-2} · sec^{-1}. The numerical and empirical data in Fig. 3 on the critical vapor contents as a function of q_w at pressure 49 bar are also instructive. The empirical data points 1, 2, and 3 correspond to w = 500, 1000, and 1900 kg · m^{-2} · sec^{-1}. The filled-in points were obtained on an experimental heated interval of length l = 1.5 mm, and the hollow data points were obtained on an experimental heated interval of length l = 3 m.

It is clear from Fig. 2 that the experimental data on the critical vapor contents at fixed p and fixed w, and increasing x_{10}, begin to increase appreciably from some value $x_{10} = x_{\Delta p}$ (in Fig. 2, these values

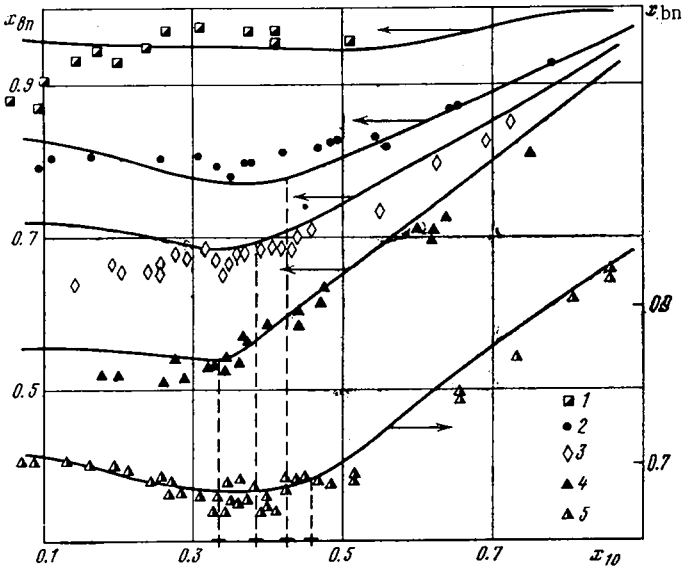

Fig. 2

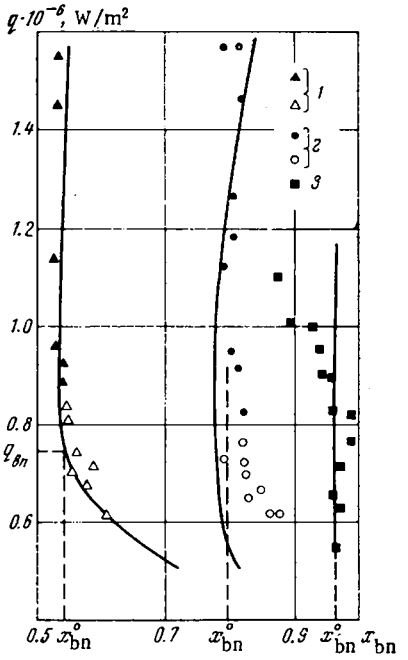

Fig. 3

are marked by a cross on the abscissa axis), while only those x_{bn} values that are independent of x_{10} are indicated in Fig. 3, to illustrate the effect of q_w alone. It is clear from Fig. 3 that there exists a sufficiently broad region over which q_w varies and within which q_w is virtually without effect on x_{bn} (the value x_{bn}°). This is due [11] to the absence of any separating out of droplets from the core of the stream onto the film of liquid. Droplets settle out at relatively low $q_w < q_{bn}$ (Fig. 3), when the transverse stream of vapor from the film, which acts to prevent droplets from settling out and is directly proportional to q_w, declines. In that case the value of x_{bn} increases by an amount Δx_2, which equals the increment in the relative rate of liquid flow through the film on account of settling of droplets.

Consequently, when $q_w \geq q_{bn}$, there is no change in the rate of liquid flow through the film on account of stripping of moisture and evaporation. The intensity of evaporation is found from Eq. (1.5). The constants $\varkappa$, n, and m in Eq. (1.6) can be estimated on the basis of the experimental value of x_{bn}, the value of x_{10}, the specific heat flux q_w, and from the solution of the inverse problem, and Eq. (1.6) can also be used to find the onset of settling out of droplets onto the film, i.e., the constant η in Eq. (1.4). The initial moisture distribution at the entry to the unheated interval is specified. For example, it is assumed that all of the liquid is distributed uniformly over the channel cross section – this condition simulated the liquid distribution after throttling at the entry to the unheated section of the experimental arrangement. Further on, the constants $\varkappa$, n, and m are so chosen as to get the numerical and empirical values of x_{bn} into close agreement.

This procedure was followed in [1] and $\varkappa$, n, and m were determined empirically at p = 49 bar, w = 1900 kg·m^{-2}·sec^{-1}, D = 8 mm, x_{10} = 0.27, $q_w = 1.21 \cdot 10^6$ W·m^{-2}, $x_{bn} = 0.54$; on the basis of empirical data [12] for p = 98 bar, w = 2100 kg·m^{-2}·sec^{-1}, D = 8 mm, $x_{10} = 0.235$, $q_w = 6.2 \cdot 10^5$ W·m^{-2}, $x_{bn} = 0.37$. The values of the constants were found to be $\varkappa = 10^{-5}$, n = −1.0, m = −0.25, η = 1.8. Subsequent numerical integration of the system of equations (1.1) demonstrated that the predicted and empirical x_{bn} values for different p, w, D, and q_w (a multiplicity of empirical data furnished by different authors on x_{bn} for p ≥ 40 bar have been collected in [3]) agree satisfactorily in the region p ≥ 45 bar. When p < 45 bar, we have $\varkappa = 10^{-7}$, n = 1.0, m = −0.25, and we obtain, from the condition that numerical and empirical x_{bn} values coincide at p = 16 bar, v = 1000 kg·m^{-2}·sec^{-1}, D = 8 mm, $x_{10} = 0.24$, $q_w = 1.02 \cdot 10^6$ W·m^{-2}, $x_{bn} = 0.63$.

Lack of agreement between the parameters at p ≥ 45 bar and at p < 45 bar shows that Eqs. (1.2) do not accurately take into account the effect of pressure on the intensity of dynamical stripping.

It is evident from Fig. 2 that the numerical and empirical x_{bn} data agree satisfactorily. When $x_{10} > x_{\Delta p}$, x_{bn} is affected by x_{10}. At low x_{10} values, we encounter numerical x_{bn} values somewhat higher than their empirical counterparts at elevated pressures (see curves 1, 2, 3, and 4). This seems to stem from a failure to take bubble entrainment of moisture from the film into cognizance. High q_w values were re-

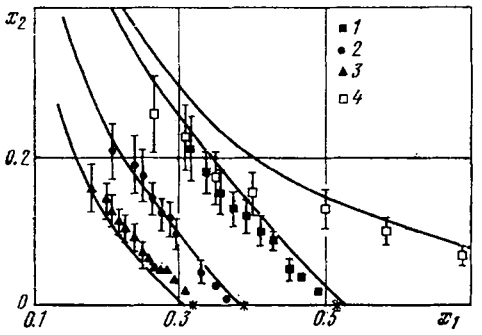

Fig. 4

quired in order to achieve burnout ($x_2 = 0$) on a heated section of restricted length when x_{10} values were low in the experiments. As noted earlier, the intensity of bubble entrainment rises markedly as q_w increases.

We also realize from Fig. 3 that, given the same q_w values in the region of high q_w values, the discrepancy between the predicted and empirical x_{bn} values is greater when the specific rates of mass flow of the mixture are smaller, i.e., when film thicknesses are greater [1]. It was also shown [4] that increased film thickness entails appreciably higher intensity of bubble entrainment. When pressures are lower (see curve 5, Fig. 2), with high velocities on the part of the components of the mixture, the empirical x_{bn} values vary inversely with x_{10} and directly with q_w accordingly. The reason for that is that the velocities of the components of the mixture are substantially greater at low pressures, given the same values of w, while the surface tension of the liquid is also much higher and the film thicknesses smaller. This hinders bubble entrainment of moisture from the film, i.e.,it hinders premature exhaustion of the film. At higher q_w values, with other conditions unchanged, the length over which dynamical stripping of moisture from the surface of the film takes place becomes shorter, and that can have the effect of decreasing the total amount of fluid stripped from the film. The liquid evaporates at a faster rate then than it is stripped from the surface of the film. That results in higher x_{bn} values at higher q_w values.

Figure 4 compares values of the relative liquid flowrate through the film x_2, obtained numerically, and direct empirical data [7, 13], where the rates of liquid flow through the film are measured as functions of w, x_1, and q_w at p = 69 bar, D = 12.6 mm at a distance of 290 D from the tube inlet. The points 1, 2, 3 correspond respectively to w = 1350, 2040, and 2700 $kg \cdot m^{-2} \cdot sec^{-1}$, and were obtained in a heated tube [7], while q_w varied over the range from $7.25 \cdot 10^5$ to $1.45 \cdot 10^6$ $W \cdot m^{-2}$. Points 4 were obtained at w = 1350 $kg \cdot m^{-2} \cdot sec^{-1}$ in an unheated tube [13]. Analysis of the empirical data shows that these were obtained roughly to within ±20%. Calculations for a heated channel were performed at inlet vapor content $x_{10} = 0.1$ with equilibrium parameters as the initial data, and the remaining conditions the same as in the experiments. Numerical results obtained in an unheated tube correspond to the equilibrium state of the system. It is clear from Fig. 4 that the results of the calculations agree closely with the empirical data.

Figure 5 displays results of calculations and experiments [8] pertaining to liquid film thicknesses in a heated tube and in an unheated tube at p = 69 bar, as functions of x_1, w, D, q_w. The film thicknesses were measured by an electric probe at a distance of 145 D (Z = 92) from the tube inlet D = 10.2 mm, and at a distance of 74 D (Z = 47) in the case of a D = 20.9 mm tube. The average liquid film thickness was determined as the distance separating the electric probe and the tube wall at which the lower limit of pulsations in the tension drop would be close to the value of the tension drop corresponding to a layer of mist, while pulsations revealing contact with the liquid would take up ~50% of the total time of contact. This last constraint is associated with the fact that irregular undulating motion takes place on the surface of the film. The results obtained in the experiments can be interpreted as measurements of average film thicknesses. In Fig. 5 we have the data points: 1) w = 1080 $kg \cdot m^{-2} \cdot sec^{-1}$, D = 10.2 mm, $q_w = 0$; 2) w = 1080 $kg \cdot m^{-2} \cdot sec^{-1}$, D = 10.2 m, $q_w \neq 0, x_{10} = 0.16$ 0.48; 3) w = 1080 $kg \cdot m^{-2} \cdot sec^{-1}$, D = 10.2 mm, $q \neq 0$, underheated; 4) w = 2700 $kg \cdot m^{-2} \cdot sec^{-1}$, D = 10.2 mm, $q_w \neq 0, x_{10} = 0.07$; 5) w = 1080 $kg \cdot m^{-2} \cdot sec^{-1}$; D = 20.9 mm; $q_w \neq 0$, $x_{10} = 0.18$ to 1.26; 6) w = 1080 $kg \cdot m^{-2} \cdot sec^{-1}$; D = 20.9 mm, $q_w \neq 0$, $x_{10} = 0.48$.

Analysis of the empirical data shows that these were found to within roughly ±20%. The calculations of the corresponding film thicknesses (see curves 1, 2, 4, 5, and 6) were carried out for the stated experimental conditions. As in the experiments, the initial data here were the parameters corresponding to the annular flow pattern, i.e., with all of the liquid concentrated in the film, and slip between phases equal to 2. Curve 3 differs from curve 2 in that it was plotted for fixed $q_w = 7 \cdot 10^5$ $W \cdot m^{-2}$.

We see clearly in Fig. 5 that the numerical and empirical data on average film thicknesses agree satisfactorily and only at relatively modest w and x_1 values do the empirical data lie below the predicted data, apparently because of the presence of an appreciable quantity of vapor bubbles in the film.

Figure 6 affords a comparison of numerical and empirical data [14] on the true vapor contents by volume φ as functions of x_1, w, q_w at p = 69 bar, D = 7.7 mm at a distance of 53 D (Z = 34) from the entry to the heated tube. The volume content of vapor was measured with the aid of a broad bremsstrahlung beam. Data points 1, 2, 3 correspond respectively to w = 800, 2000, 3000 $kg \cdot m^{-2} \cdot sec^{-1}$. The cluster of

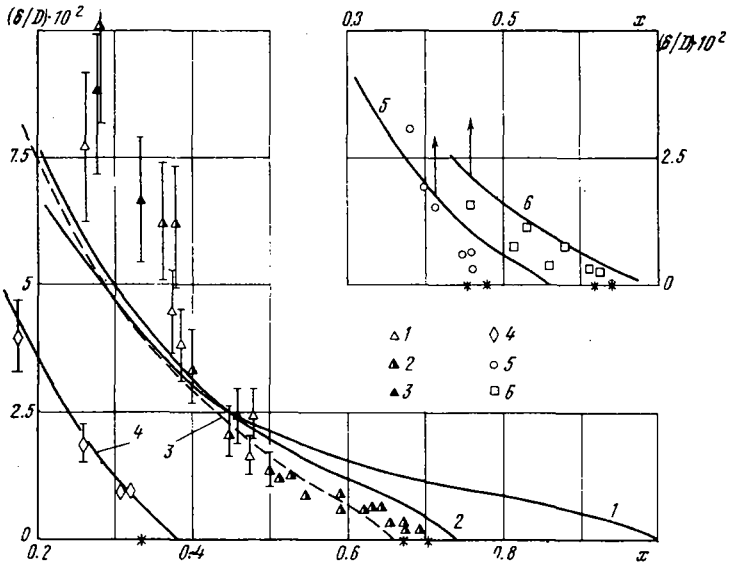

Fig. 5

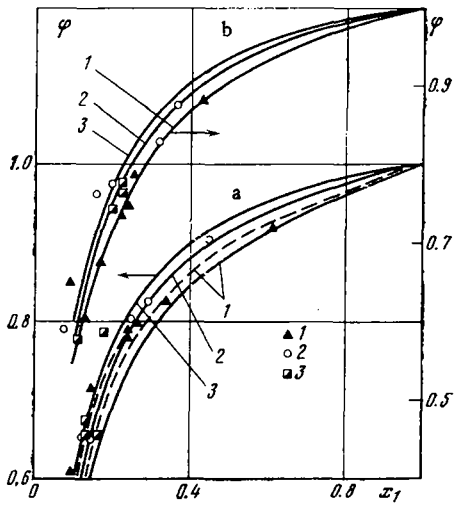

Fig. 6

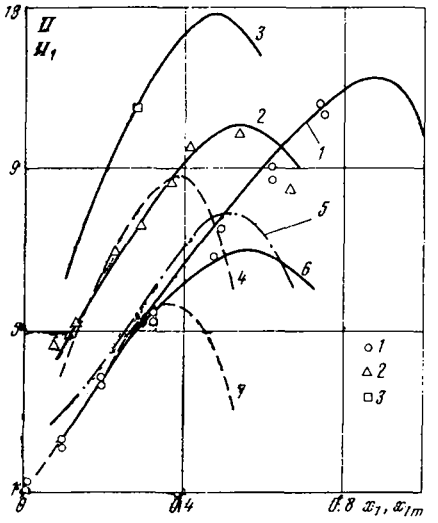

Fig. 7

data points designated *a* was obtained in the unheated tube, while the cluster of data points designated b was obtained at $q_w = 1.16 \cdot 10^6$ W·m^{-2}. The maximum absolute error in the determination of φ was ±5%. Calculations were carried out for Z = 0 in the case of flow of a mixture through an unheated tube; all of the liquid was found in the core of the stream (simulation of a throttling globe valve in the experimental arrangement). The continuous curves are referable to the equilibrium state of the system, while the dashed curves correspond to data for the cross section located at a distance of 140 D (Z = 90) from the initial cross section. The data for this cross section were taken as the initial data at the entry to the heated section.

It is evident in Fig. 6 that the predicted data and numerical data fit closely within the limits of experimental error. Note that the spread of empirical data points does not allow us to ascertain the effect of w on φ, which stems from the results of the numerical calculations.

Figure 7 shows examples of results of calculations and experiments [16] on hydraulic drag for flow of a steam–water mixture through a smooth horizontal tube and smooth vertical tube as functions of x_1 and q_w at p = 98 bar, w = 1000 kg·m^{-2}·sec^{-1}. The inner diameter of the horizontal part of the tube is 11.1 mm, that of the vertical part is 8 mm. Three pressure taps were set on the horizontal run. The distance separating the first and third tap is 3 m, and that separating the second and third tap was 0.55 m. On the vertical run, the distance between pressure taps was 0.6 m. We note these intervals between pressure taps as *a*, b, and c, respectively. The relative pressure losses due to friction II and the analogous ratio

of pressure losses Π_i (due to friction and to acceleration of the phases and equal to the ratio of pressure losses in two-phase flow due to friction and acceleration of phases) to the pressure losses due to friction alone in flow of water at saturation temperature with the same specific mass flowrate, is plotted as the vertical in Fig. 7:

$$\Pi_i = \left[\frac{dp}{dz}\right]_f + \left[\frac{dp}{dz}\right]_a \Big/ \left[\frac{dp}{dz}\right]_l$$

We have $\Pi_1 = \Pi$ in the equilibrium state of the system in the tube. The empirical data points 1 in Fig. 7, with reference to Π, were obtained on intervals *a* and b in the absence of heating. The empirical data points 2 for Π_1 were obtained on interval b at $q_w = 5.83 \cdot 10^5$ W · m^{-2} as a function of the average $x_{1m} = (x_{10} + x_{1e})/2$, where x_{1e} is the flow vapor content at the exit from the heated section. The vapor content increment on this interval $\Delta x = x_{1e} - x_{10} = 0.085$. Empirical data point 3 for Π_1 was obtained on the interval such that $q_w = 1.16 \cdot 10^6$ W · m^{-2}. The empirical data points 2 were used in calculating the dependence of the relative pressure losses due to friction Π on x_{1m} [14] (see curve 5). Curve 1 is plotted numerically for the case of flow of the mixture through an unheated tube in the equilibrium state of the system. Curves 2 and 6 are plotted for the experimental conditions, i.e., using numerical data on the pressure drop and on x_{1m} on the interval b to construct the dependences of Π and Π_1 on x_{1m}. Curve 3 (giving the dependence of Π_1 on x_1 at $q_w = 1.16 \cdot 10^6$ W · m^{-1}) and curves 4 and 7 (giving the dependences of Π and Π_1 on x_1 at $q_w = 5.83 \cdot 10^5$ W · m^{-2}) were plotted for feed of a mixture such that $x_{10} = 0.1$ to the tube inlet.

Figure 7 makes it clear that, starting with a certain value x_1 (or Z in the heated tube, Fig. 1), the increase slows down and the relative pressure drops diminish. The hydraulic drag reaches its critical point. As x_{10} increases, the critical point of the hydraulic drag shifts toward higher x_1 values (as we clearly realize from comparing curves 2 and 4). Numerical calculations based on that model showed that the phenomenon of critical hydraulic drag is due in the main to the combined effect of two factors: on the one hand, with increasing x_1 slip between the vapor and the liquid film increases [1], so that friction between the vapor and film likewise increases, while on the other hand, the increase in x_1 is accompanied by a decrease in the thickness of the film and as a consequence a decrease in the roughness of the film, and that in turn entails less friction between the vapor and the film. The twofold influence exerted by x_1 results in the appearance of critical hydraulic drag. We infer from a comparison of curve 1 with curves 6 and 7 that q_w exerts only a negligible effect on Π in the region prior to the critical hydraulic drag.

We also infer from the above discussion that simulation of the flow of mixture through real steam-generating tubes in which water underheated up to saturation temperature, or a water–steam mixture of low steam content x_1, is fed to the inlet of the tubes, by short experimental sections with feed of mixture to the inlet at different x_{10} values, can be achieved only up to a certain fully specified value of x_{10} (see curves 2 and 4 in Fig. 7). Otherwise the effect of x_{10}, say on x_{bn}, Π, Π_1, will begin to be felt. That means that a sufficiently long unheated interval [1] on which the equilibrium state of the system would be attained would have to be provided ahead of the heated section.

LITERATURE CITED

1. B. I. Nigmatulin, "Hydrodynamics of two-phase flow in dispersed annular flow pattern," Zh. Prikl. Mekhan. i Tekh. Fiz., No. 6 (1971).
2. V. E. Doroshchuk and B. I. Nigmatulin, "Burnout of the second kind in a vertical tube at moderately high pressures," Teploénergetika, No. 3 (1971).
3. V. E. Doroshchuk, Burnout in Boiling of Water in Tubes [in Russian], Énergiya, Moscow (1970).
4. V. I. Petrovichev, L. S. Kokorev, A. Ya. Didenko, and G. G. Dubrovskii, "Droplet entrainment in boiling of thin films of liquid," in: Topics in Nuclear Reactor Heat Transfer Studies, No. 2 [in Russian], Atomizdat, Moscow (1970).
5. G. F. Hewitt, H A. Kearsey, P.M. C. Lacey, and D. J. Pulling, "Burnout and nucleation in climbing film flow," AERE-R4374, Harwell (1963).
6. I. I. Paleev and B. S. Philipovich, "Phenomena of liquid transfer in two-phase dispersed annular flow," Internat. J. Heat and Mass Transfer, 9, No. 10 (1966).
7. A. W. Bennett, G. F. Hewitt, H. A. Kearsey, R.K.F. Keeys, and R. A. Stinchcomber, "Measurement of liquid film flow rates at 1000 psia in upward steam water flow in vertical heated tube," AERE-R5809, Harwell (1969).
8. A. E. Bergles and J. P. Roos, "Film thickness and critical heat flux observations for high pressure water in spray annular flow," Internat. Symposium on Res. in Cocurrent Gas–Liquid Flow, Vol. 2 (1968).

9. R. Staniforth, G. F. Stevens, and R. W. Wood, "An experimental investigation into the relationship between burnout and film flow rate in a uniformly heated round tube," AEEW-R430 (1965).
10. Yu. I. Dzarasov, B. A. Kol'chugin, and E. I. Liberant, "Experimental investigation of characteristics of heated two-phase flow," Heat Transfer and Mass Transfer [in Russian], Vol. 2, Part 1, Minsk (1972).
11. V. E. Doroshchuk, L. I. Levitan, and B. I. Nigmatulin, "Development of conditions for settling out of droplets from the core of a disperse flow onto a liquid film in a heated tube," in: Proceedings of the 9th All-Republic intercollegiate conference on vaporization, combustion, and gas dynamics of disperse systems [in Russian], Odessa Univ. Press, Odessa (1969).
12. A. S. Kon'kov, "Experimental investigation of conditions for deterioration of heat transfer in the flow of a steam–water mixture through heated tubes," in: Trudy TsKTI, No. 58 (1965).
13. R. K. F. Keeys, J. C. Ralph, and D. N. Roberts, "Liquid entrainment in adiabatic steam–water flow at 500 and 1000 psia, AERE-R6293 (1970).
14. Z. L. Miropol'skii and R. I. Shneerova, "Investigation of the phase composition of a water–steam mixture in a heated tube with the aid of bremsstrahlung," Teplofiz. Vys. Temp., 1, No. 1 (1963).
15. N. V. Tarasova, "Hydraulic drag in boiling of water and of a water–steam mixture in heated tubes and in annular channels," Trudy TsKTI, No. 59 (1965).